Experimental investigation of promontory motion and intracranial pressure following bone conduction: Stimulation site and coupling type dependence

Dobrev, Ivo ; Sim, Jae Hoon ; Pfiffner, Flurin ; Huber, Alexander M ; Röösli, Christof

Abstract: Objective Investigation of bone conduction sound propagation by osseous and non-osseous pathways and their interactions based upon the stimulation site and coupling method of the actuator from a bone conduction hearing aid (BCHA). Methods Experiments were conducted on five Thiel embalmed whole head cadaver specimens. The electromagnetic actuator from a commercial bone conduction hearing aid (BCHA) (Baha® Cordelle II) was used to provide a stepped sine stimulus in the range of 0.1–10 kHz. Osseous pathways (direct bone stimulation or transcutaneous stimulation) were sequentially activated by stimulation at the mastoid or the BAHA side using several methods including a percutaneously implanted screw, Baha® Attract transcutaneous magnet and a 5-N (5-N) steel headband. Non-osseous pathways (only soft tissue or intra-cranial contents) were activated by actuator stimulation on the eye or neck via attachment to a 5-N steel headband, and were compared with stimulation via equivalent attachment on the mastoid and forehead. The response of the skull was measured as motions of the ipsi- and contralateral promontory and intracranial pressure (ICP) in the central, anterior, posterior, ipsilateral and contralateral temporal regions of the cranial space. Promontory motion was monitored using a 3-dimensional Laser Doppler vibrometer (3D LDV) system. Results The promontory undergoes spatially complex motion with similar contributions from all motion components, regardless of stimulation mode. Combined 3D promontory motion provided lower inter-sample variability than did any individual component. Transcranial transmission showed gain for the low frequencies and attenuation above 1 kHz, independent of stimulation mode This effect was not only for the magnitude but also its spatial composition such that contralateral promontory motion did not follow the direction of ipsilateral stimulation above 0.5 kHz. Non-osseous stimulation on the neck and eye induced comparable ICP relative to percutaneous (via screw) mastoid stimulation. Corresponding phase data indicated lower phase delays for ICP when stimulation was via non-osseous means (i.e., to the eye) versus osseous means (i.e., to the mastoid or forehead). Sound propagation due to skull stimulation passes through the thicker bony sections first before activating the CSF. Conclusion Utilization of 3D promontory motion measurements provides more precise (lower inter-sample variability) information about bone vibrations than does any individual component. It also provides a more detailed description of transcranial attenuation. A comprehensive combination of motion and pressures measurements across the head, combined with a variation of the stimulation condition, could reveal details about sound transmission within the skull.

DOI: https://doi.org/10.1016/j.heares.2019.03.005

Originally published at:
Dobrev, Ivo; Sim, Jae Hoon; Pfiffner, Flurin; Huber, Alexander M; Röösli, Christof (2019). Experimental investigation of promontory motion and intracranial pressure following bone conduction: Stimulation site and coupling type dependence. Hearing Research, 378:108-125.
DOI: https://doi.org/10.1016/j.heares.2019.03.005

Research Paper

Experimental investigation of promontory motion and intracranial pressure following bone conduction: Stimulation site and coupling type dependence

Ivo Dobrev[a, b, *]

ivo.dobrev@usz.ch

Jae Hoon Sim[a, b]

Flurin Pfiffner[a, b]

Alexander M. Huber[a, b]

Christof Röösli[a, b]

[a]Department of Otorhinolaryngology, Head and Neck Surgery, University Hospital Zürich, Zürich, Switzerland

[b]University of Zürich, Zürich, Switzerland

[*]Corresponding author. Department of Otorhinolaryngology, Head and Neck Surgery, University Hospital Zürich, Frauenklinikstrasse 24, CH-8091, Zürich, Switzerland.

Abstract

Objectives

Investigation of bone conduction sound propagation by osseous and non-osseous pathways and their interactions based upon the stimulation site and coupling method of the actuator from a bone conduction hearing aid (BCHA).

Methods

Experiments were conducted on five Thiel embalmed whole head cadaver specimens. The electromagnetic actuator from a commercial bone conduction hearing aid (BCHA) (Baha® Cordelle II) was used to provide a stepped sine stimulus in the range of 0.1–10 kHz. Osseous pathways (direct bone stimulation or transcutaneous stimulation) were sequentially activated by stimulation at the mastoid or the BAHA side using several methods including a percutaneously implanted screw, Baha® Attract transcutaneous magnet and a 5-N (5-N) steel headband. Non-osseous pathways (only soft tissue or intra-cranial contents) were activated by actuator stimulation on the eye or neck via attachment to a 5-N steel headband, and were compared with stimulation via equivalent attachment on the mastoid and forehead. The response of the skull was measured as motions of the ipsi- and contralateral promontory and intracranial pressure (ICP) in the central, anterior, posterior, ipsilateral and contralateral temporal regions of the cranial space. Promontory motion was monitored using a 3-dimensional Laser Doppler vibrometer (3D LDV) system.

Results

The promontory undergoes spatially complex motion with similar contributions from all motion components, regardless of stimulation mode. Combined 3D promontory motion provided lower inter-sample variability than did any individual component. Transcranial transmission showed gain for the low frequencies and attenuation above 1 kHz, independent of stimulation mode This effect was not only for the magnitude but also its spatial composition such that contralateral promontory motion did not follow the direction of ipsilateral stimulation above 0.5 kHz. Non-osseous stimulation on the neck and eye induced comparable ICP relative to percutaneous (via screw) mastoid stimulation. Corresponding phase data indicated lower phase delays for ICP when stimulation was via non-osseous means (i.e., to the eye) versus osseous means (i.e., to the mastoid or forehead). Sound propagation due to skull stimulation passes through the thicker bony sections first before activating the CSF.

Conclusion

Utilization of 3D promontory motion measurements provides more precise (lower inter-sample variability) information about bone vibrations than does any individual component. It also provides a more detailed description of transcranial attenuation. A comprehensive combination of motion and pressures measurements across the head, combined with a variation of the stimulation condition, could reveal details about sound transmission within the skull.

Keywords: Bone conduction pathways; 3D laser Doppler vibrometry; Cadaver head; Promontory motion; Intracranial pressure; Soft-tissue stimulation

1 Introduction

Bone conduction (BC) is a normal pathway for sound to reach the inner ear. The sensation is similar or equal to that resulting from stimulation by air conduction (AC) (von Békésy, 1932; Stenfelt, 2007). Several different pathways of sound transmission have been described (von Békésy, 1932; Bárány, 1938; Stenfelt and Goode, 2005b; Stenfelt, 2015; Tonndorf and Khanna, 1968). The contribution of each of these pathways to the final sensation of hearing is still a matter of debate.

In clinical evaluations of hearing, BC testing with stimulation by tuning forks or by pure-tone audiometry is an important diagnostic method to differentiate between a conductive, sensorineural and mixed hearing loss (Hulecki and Small, 2011). Further, bone conduction hearing aid (BCHA) treatment has become the standard of care for patients suffering from conductive or mixed hearing losses who cannot wear conventional hearing aids, and for patients with single-sided deafness (SSD) (Pfiffner et al., 2011). In patients with SSD, sound needs to travel from the site of stimulation to the contralateral cochlea. The loss of sensitivity between stimulation and contralateral sensation is called transcranial attenuation. Transcranial attenuation is important in many aspects of hearing and in interpreting numerous clinical tests. For example, it defines the amount of masking necessary for measuring BC thresholds (Hood, 1960; Studebaker, 1964). The population averages of different data sets of transcranial attenuation for a bone conducted signal vary considerably ranging from 0 to 15 dB in the frequency range of 0.25–4 kHz, while intra-individual variations are even larger (Hurley and Berger, 1970; Snyder, 1973, Nolan and Lyon, 1981). One of the considered pathways is based on the interactions between the skull and non-osseous contents of the skull, such as the cerebrospinal fluid (CSF), causing intracranial pressure changes (Röösli et al., 2016). The sound may be transmitted via the internal auditory canal or the aqueducts to the inner ear fluid (See Fig. 1, #4), resulting in a pressure difference across the basilar membrane (Sohmer et al., 2000; Sohmer and Freeman, 2004; Adelman et al., 2012; Perez et al., 2011). The role of this pathway for perception of sound is currently unclear.

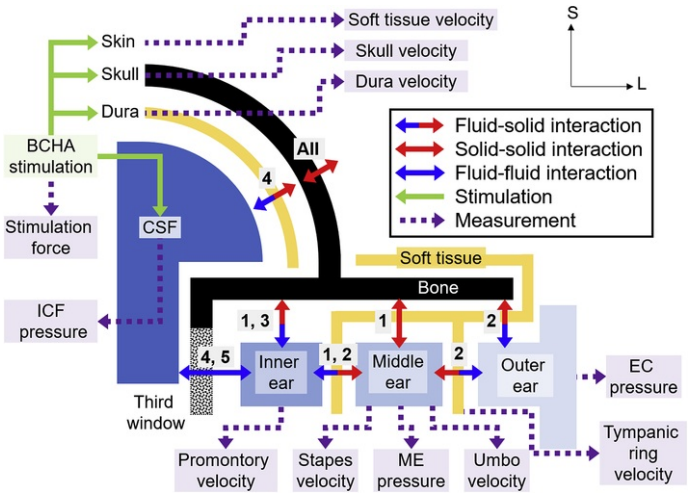

Fig. 1 Simplified scheme of the human head, with corresponding interface boundaries and interaction types among all components involved in bone conduction. Interaction types, with corresponding boundaries, for the five BC pathways are enumerated.

alt-text: Fig. 1

Some BCHA stimulate on the skin covered skull, whereas others stimulate directly on the skull, either via direct attachment (Håkansson et al., 2010) or by attachment to an implanted screw. While previous research (Stenfelt, 2012) has shown dependence of transcranial attenuation on stimulation location, large intersample variability has prevented statistically stronger and more detailed conclusions, such as potential dependence on mode of stimulation (coupling type) as well as location. Besides stimulation on the skull or skin covered bone (osseous), stimulation on soft tissue (non-osseous) such as the eye, neck or thorax (i.e., soft-tissue stimulation) can cause a hearing sensation. For example, distortion product otoacoustic emissions can be elicited by a combination of an air-conducted stimulus presented via an earphone in the ear canal and a stimulus on the eye delivered via a BC actuator (Watanabe et al., 2008) or via direct stimulation on the dura (Stump et al., 2018). Soft-tissue stimulation is a potential additional pathway contributing to sound transmission in a high-energy sound field, particularly above 1 kHz, where the head undergoes deformations. These in turn could excite the intracranial fluid directly through the skull bone, via the spinal cord or other potential pathways. This could have implications for ear protection in high noise environments, such as an explosion. Using only earplugs or earmuffs would limit protection to approximately 38–43 dB from 1 to 1.4 kHz (Ravicz et al., 2000), or it may be frequency dependent, ranging from 40 to 60 dB (Reinfeldt et al., 2007).

Measurements of promontory motion have been accepted for estimating BC hearing sensation (Stenfelt and Goode, 2005a; Eeg-Olofsson et al., 2008, 2013; Dobrev and Sim, 2018; Stenfelt et al., 2004a,b(This should be Stenfelt et al 2004 - without "a,b" as there is only one reference from 2004. There are two references from 2005, but they are not referenced here.)). Levels of vibration of the cochlea in cadaver heads are similar to those measured in the live human (Eeg-Olofsson et al., 2013). However, there are large interindividual variations of the correspondence of level of vibration and hearing perception. This may have been due in part to use of a LDV system with only one sensitivity axis. Thus, 3D motion needs to be considered because the magnitude and phase of the maximum velocity vector of cochlear promontory motion could be a better descriptor of BC hearing than individual orthogonal components of promontory motion (Dobrev and Sim, 2018).

In general, further research is needed to define the dependence of bone conduction transmission on the location of stimulation and the method of coupling of the BCHA actuator (Ito et al., 2011; Stenfelt, 2012; Röösli et al., 2016; Sim et al., 2016). Thus, the overall goal of the current experiments is to describe further the significance and interaction between different pathways for transmission of vibrations from a BCHA actuator applied to bone or soft tissue. The specific aims are to analyze 1) 3D motion of the promontory following BC stimulation, 2) its dependence on the method of coupling (coupling type) of the BCHA actuator, 3) propagation of intracranial pressure (ICP) as a function of different modes of promontory activation, and 4) comparison of intracranial pressure and promontory motion for different modes of stimulation. We hypothesize that 1) the mode of stimulation affects transcranial attenuation, 2) sound could be transmitted to the cochlea via intracranial contents independent of osseous pathways, and 3) this fluid pathway depends on the mode of stimulation.

2 Methods

This study was approved by the Ethical Committee of Zürich (KEK-ZH-Nr. 2012-0136).

2.1 Measurement procedure

The response of each cadaver head to a BC stimulus was experimentally evaluated by varying the position and coupling (attachment) of an BCHA actuator. Schematics of the various measurement conditions and locations, as well as coupling types are shown in Fig. 2.

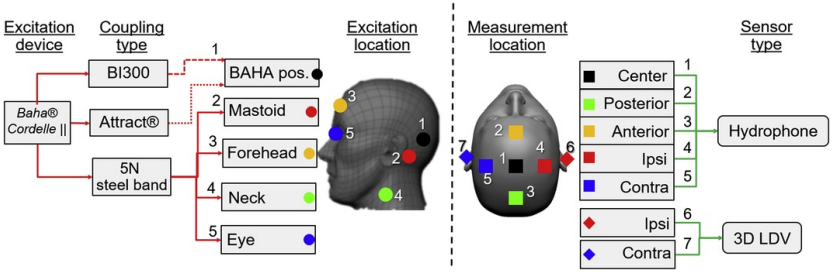

Fig. 2 A schematic overview of measurement procedure for excitation with Baha® Cordelle || at various stimulation locations and with different coupling (attachment) types. For each stimulation location and coupling type, 3D velocity and ICP were measured at several measuremen locations. Illustrated (with colors and numbers) are the approximate positions of the various excitation and measurement locations for all experiments. (For interpretation of the references to color in this figure legend, the reader is referred to the Web version of this article.)

alt-text: Fig. 2

Five stimulation locations were tested: 1) skin-covered skull at the traditional location for a bone anchored hearing aid (BAHA), i.e., 55 mm from the entrance of the ear-canal at the line extending from the lateral margin of the eye to the upper border of the pinna (Reinfeldt et al., 2014); 2) mastoid at a typical position for clinical audiometry; 3) forehead, in the midline 5 cm above the root of the nose; 4) eye, ipsilateral; 5) neck, on the sternocleidomastoid muscle approximately 5–7 cm below its insertion on the mastoid. Three coupling conditions were tested: 1) a 5-N steel headband for stimulation locations at the mastoid, forehead, eye and neck; 2 and 3) BI 300 and Baha Attract® (Cochlear® BAS, Mölnlycke, Sweden), respectively, for the BAHA position.

The response of each cadaver head under each measurement condition was evaluated using measurements of the combined velocity of the ipsi- and contralateral promontory, measured sequentially, and the intracranial pressure (ICP). The method for measurement of the combined velocity is described in Section 2.4 and is based on the work of Dobrev and Sim (2018). The ICP was measured at five regions within the cranial space: anterior, posterior, ipsilateral, contralateral and central. All ICP measurement locations, as indicated in Fig. 2, were distributed across a horizontal plane on the level of the forehead, approximately 5–7 cm inferior from the vertex of the skull. The promontory motion was chosen because it is an accepted estimator for the resultant hearing sensation (Eeg-Olofsson et al., 2013; Stenfelt, 2015). The ICP was recorded because it is hypothesized to be indicative of the non-osseous BC stimulation of the cochlear fluid (Sohmer and Freeman, 2004; Stump et al., 2018).

In order to reduce possible short and long-term drift in the response of the Thiel-preserved cadaver heads (Guignard et al., 2013), corresponding measurements for a given evaluation were grouped into a single measurement session executed within 1 day (<6–12 h). Two measurement sessions were executed per head: 1) evaluation of the effect of stimulation location; and 2) evaluation of the coupling type. For the evaluation of the stimulation location, the BC actuator location was sequentially moved between the mastoid, forehead, neck and eye, while the other parameters were kept constant: 1) the coupling type was kept as a 5-N steel band; 2) the promontory motion was measured on the ipsilateral side; and 3) the ICP was measured in the central region. This resulted in four consecutive measurements for this experimental evaluation. For evaluation of the coupling type, the attachment of the Baha actuator was varied sequentially, between the 5-N steel band on the mastoid, and BI300 or Attract® on the BAHA location, respectively. Since the LDV and hydrophone signals could be recorded simultaneously, the hydrophone position was iteratively cycled across the five CSF regions (shown in Fig. 2, right), while the LDV was kept at the ipsilateral promontory. The contralateral promontory was then measured while the hydrophone was kept at the central CSF region. This approach resulted in six measurements per attachment type, for a total of 18 measurements for this experimental evaluation.

All five CSF positions were initially set with x-ray in the first excitation condition, then the locations were marked on our custom positioning rig and used subsequently when moving the hydrophone. Initial preliminary tests using comparison with repeated x-ray showed about a 1-cm repeatability in the hydrophone positioning using this method.

It should be noted that the coupling on the mastoid is at a different location (approximately 2–3 cm away) than that for the BI300 and Attract®, with different underlaying bone and soft tissue structure. This could potentially lead to differences in the response of the head, not only due to coupling but also due to stimulation location. This choice of measurement procedure was made such that only clinically relevant coupling types were included. This approach also avoided the problem of having the BI300 (screw only) under the skin during on-skin stimulation (i.e., when the 5-N steel band coupling was applied at the BAHA location), or having to remove the BI300 during other coupling type measurements.

2.2 Sample preparation

The experiments were conducted on five Thiel embalmed (Thiel, 1992; Guignard et al., 2013) whole head cadaver specimens in the age range of 50–80 years. Overall sample preparation was done in a similar way to Röösli et al. (2016). Discussions of the choice of samples and their temporal stability over the length of the experimental sessions is included in Section 4.1.

In order to provide optical access to the promontory for the vibration measurements, an endaural incision was made between ascending helix and tragus, and a tympanomeatal flap was elevated to expose the promontory on both sides of the head. Two self-retaining retractors were placed to allow good visualization of both the endaural surgery and the later LDV measurement. The measurement point at the promontory, located approximately 1–3 mm from the round window, was covered with either a 1–2 mm^2 retro-reflective sticker (DG3 4000, 3M, MN, USA) or retro-reflective spheres (30–100 µm in diameter, P2453BTA-4.2 30–100 µm, Cospheric LLC, CA, USA) glued to the promontory's surface with cyanoacrylate glue (57040-00000, tesa SE, Norderstedt, Germany). The choice of retro-reflector type for each cadaver head was based on the specific anatomy and condition of the promontory's wall. Before application of the retro-reflector, the promontory area was cleaned of fat and soft tissue and dried with cotton.

In order to provide access to the CSF for ICP measurements with a hydrophone, the skull was opened at the vertex and a 10-mm diameter tube was tightly sealed to the opening. A hydrophone (Type 8103, Brüel & Kjær, Denmark) was inserted into the intracranial space through the tube. The hydrophone was positioned within the cranial volume using X-ray as guidance, while care was taken to prevent any contact with the sample and minimize any direct mechanical coupling between the hydrophone and the skull. The X-ray control was applied on the first set of measurements of each head then marked as described previously. A physiologic intracranial pressure of 15 cm-H_2O was maintained by a water column in the tube attached to the skull (Steiner and Andrews, 2006).

Coupling forces for the 5-N steel band, which was used for mastoid, forehead, neck and eye placement, were controlled with a spring gauge (10 N range, 0.1 N accuracy, Light Line, Pesola, Switzerland). For positioning of the actuator on the eye, the whole surface of the actuator pad (the connector disk of the 5-N headband) was in contact with the vitreous body without touching the bone of the orbita. In most heads, the eye ball was deflated. To compensate for that, a water bubble (~3 cm in diameter), made of a piece of latex glove, was placed between the actuator pad and the eye socket. The aim of the addition of the water bubble was to minimize direct contact between the actuator and the skull bone, while providing non-osseous connection, imitating the liquid filled eye ball. For stimulation on the BAHA location, a titanium implant (BI300) was placed into the skull bone through a percutaneous opening (slit) of 2–3 cm immediately above the implant location. Coupling to the BI300 was done sequentially by first using a transcutaneous placement via an Attract® magnet system followed by a percutaneous placement via the abutment. Skin thickness (including both skin and subcutaneous tissues) varied from 4 to 7 mm.

2.3 Measurement setup

For each stimulation location, the motions of both the ipsi- and contralateral promontories were measured sequentially by moving the 3D LDV in a repetitive manner via a robotic arm (Dobrev et al., 2017). The cadaver heads were oriented in a natural upright position, as shown in Fig. 3, similar to Dobrev and Sim (2018). With this configuration, most of the head's weight was supported by the spine, which in turn was stabilized with a short metal rod (12-mm diameter stainless steel) inserted in the spinal column of the last few inferior vertebrae of the remaining spine (~5 cm corresponding to two vertebrae). For additional support to prevent tipping of the head and potential orientational

drift during a full measurement session (i.e., 4–6 h), the cadaver heads were gently supported around the scalp with a soft band connected via rubber bands (<1 N per band), to four stiff metal rods (12–20 mm diameter stainless steel), providing gentle (<2–4 N total) lateral support. The full assembly of the head holder was supported by vibration isolation legs (Sorbothane legs, AV3, Thorlabs Inc., NJ, USA) and placed on a vibration isolation table (M-INT1-36-6-A, Newport Corp., CA, USA) to minimize random vibrations from external sources. The overall aim of the head holder was to mimic the natural orientation and support of the human head, specifically for measurements of the lower frequencies (below 0.5–1 kHz), since previous work (Hoyer and Dorheide, 1983; McKnight et al., 2013; Dobrev et al., 2017) had indicated that cadaver head motion at such frequencies is rigid-body-like, thus heavily dependent on support (boundary) conditions.

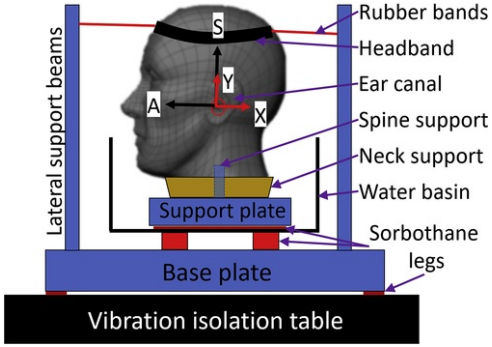

Fig. 3 Overview of the head support setup. Indicated are the anatomical and 3D LDV coordinate systems. Origin of the 3D LDV coordinate system is situated on the cochlea promontory.

alt-text: Fig. 3

The actuator of a Baha® Cordelle II (Cochlear Company, Australia) was used for excitation for all measurement conditions. It was modified to allow for direct electrical stimulation from a sound generator (APx585, Audio Precision Inc., USA) via an audio amplifier (RMX 850a, QSC, CA, USA). For each experimental condition, a frequency stepped sinusoidal stimulus was applied to the BC actuator at 81 logarithmically distributed frequencies in the range of 0.1–10 kHz, resulting in 40 frequency points per decade. The stimulus at each frequency was presented continuously for 200 ms with a sinusoidal-shaped ramp up (onset) region of 20 ms and a constant stimulation voltage of 1 Vrms.

For each stimulation frequency, the promontory motion was measured using a single point 3-dimensional (3D) LDV (3D CLV 3000 by Polytec GmbH), providing the time waveform of three orthogonal velocity components, from which the corresponding acceleration components were calculated. The orientation of the 3D LDV coordinate system relative to the anatomical coordinate system is illustrated in Fig. 3. The LDV's X-axis was pointing approximately towards the posterior direction for measurements at the ipsilateral promontory and approximately towards the anterior direction for measurements at the contralateral promontory. The Z-axis was pointing laterally (away) from the promontory, and the Y-axis was always pointing in the superior direction for both ipsi- and contralateral measurements.

2.4 Data processing

To reduce effects from random external disturbances, such as LDV signal drop, measurements at each frequency were repeated five times. Several types of quality checks were applied to each data set (five iterations) at each frequency to determine which data were to be further used, similar to Dobrev et al. (2017): 1) signal-to-noise ratio (SNR) of at least 2 standard deviations above the average noise floor in the vicinity (in the frequency domain) of each stimulus frequency (Dobrev et al., 2018a); 2) amplitude repeatability within 20%, based on the complex vector difference (complex vector in the frequency domain) between any of the iterations, at a particular frequency, and the geometric average of the magnitudes of all iterations; 3) coherence of more than 0.85, where the coherence for each iteration was calculated for the waveform of each LDV channel and the stimulus signal. After the application of all three data quality criteria, the remaining data (if available) from the set of five iterations per frequency was reduced to one averaged data point (complex number) per frequency, based on the medians of the real and imaginary parts of the iterations meeting the quality criteria. Since data from five cadaver heads were obtained, the results for each measurement condition (stimulation location, promontory side, etc.) were averaged across heads, only for data meeting the quality criteria. Averaging of the magnitudes was based on the geometric mean and averaging of phases was based on the median. The geometric mean was applied on the data in the linear scale and was chosen due to the better fit of the intersample data to a log-normal distribution indicated by a Lilliefors test (explained in Section 2.5). Similar results and observations could have been obtained by taking the mean (or median) of the magnitude data in the logarithmic (dB) scale.

Since all three Cartesian components of the velocity were measured, the combined velocity was calculated based on methods described previously (Dobrev et al., 2017; Dobrev and Sim, 2018). The combined velocity was defined as the maximum magnitude of the complex vectoral sum of the three individual components (Dobrev and Sim, 2018). This method accounts for both the spatial (magnitudes and directions) and temporal (phases) of the individual

Cartesian components. The noise floor of the combined motion was calculated from the noise floors of the individual components based on their magnitudes only, as the phase of the noise data is meaningless within the scope of this paper. The combined velocity was chosen, instead of any individual motion component, since it provided a single value instead of three, which made interpretation simpler. In addition, from a physiological perspective, the combined velocity is indicative of the total vibratory motion and corresponding total kinetic energy at a given measurement point (Dobrev and Sim, 2018; Stenfelt and Goode, 2005a). Accordingly, the combined motion is assumed to be a better representative of the perceived sound (i.e., closer to hearing sensation), compared to any of the individual components alone (Stenfelt and Goode, 2005a).

Data for the driving force of the actuator were not available in our tests, thus corresponding promontory motion was normalized by the driving voltage of the actuator. This was done for all promontory motion data in this work. This could have introduced potential variations in the data due to variations in local point impedances as seen by the actuator, thus potentially resulting in different forces at different locations and coupling types.

All post-processing, analysis and data representation was done via custom MATLAB scripts (MATLAB 2017a, MathWorks, MA, USA).

2.5 Statistical methods

A paired-sample *t*-test was used to estimate the statistical significance of the differences in the promontory response (both magnitude and phase) due to any two measurement parameters (stimulation location, motion components, effect of mastoidectomy) within a specific frequency range. All statistical tests were two-tailed. In addition, the confidence interval for difference between any two measurement data sets was estimated based on the assumption of a normal distribution of the data. Normal distribution of the data set (logarithmic scale) was tested with a Lilliefors test (Lilliefors, 1967) for both the confidence interval and statistical significance. A p-value of <0.05 was used as a threshold for statistical significance for all tests. Since only 5 samples were available for this study per frequency point, data at all frequencies within a specified frequency band were used for comparison, rather than at individual frequencies. This was done by averaging the response of each head across all frequencies in the particular frequency band and using the resultant in the statistical tests as a representative of the individual head response. This yielded more robust data (i.e., less effect of notches or peaks varying between samples) for the statistical evaluation of the significance of any potential differences within a given frequency band of interest. There were five frequency bands under consideration, equally distributed across the frequency range of 0.1–10 kHz with an approximate width of 1 octave each. These five bands were used to represent the overall response at low (0.1–0.2 kHz), low-mid (0.25–0.56 kHz), mid (0.67–1.5 kHz), mid-high (1.7–3.8 kHz) and high (4.5–10 kHz) frequencies.

Within each band, several statistical calculations, as illustrated in Fig. 4, were performed on the magnitude (in dB) and phase (in cycles) data for each measurement condition. Per-frequency average was calculated as the median of the individual data at each individual frequency. Band average was calculated as the median of the per-frequency averages at all frequencies within the specific frequency band. While the band average was a single value for each band, it was plotted as a line (see example in Fig. 4), the length of which represented the width of the band. An upper and lower bound for a 95% confidence interval (assuming a normal distribution) was calculated based on the average (median) response of each individual sample within the specific frequency band. Statistical significance ($p < 0.05$) of the difference between a given measurement condition and a reference measurement condition (displayed in black on all figures) was evaluated based on a paired-sample *t*-test and marked with an "X" on the center of the band. This representation scheme allowed display of both the per-frequency behavior as well as the band-averaged response and statistical outcomes for each measurement condition for illustration purposes.

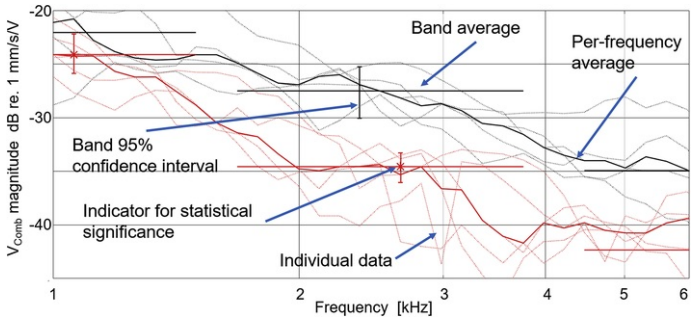

Fig. 4 Overview of data processing done per frequency and within each frequency band, including averaging across samples and frequencies, confidence interval estimation, and evaluation of statistical significance.

alt-text: Fig. 4

It should be noted that no adjustment was applied for the use of multiple t-tests (~250 times across the data set). Due to the small sample size ($n = 5$), no further statistical analysis or corrections were done. Thus the uncorrected *t*-test results are indicative of potential trends in the comparisons rather than rigorous statistical proof of significant difference. In future work, if more samples are obtained, a more rigorous statistical analysis could be applied, such as, for example, a repeated measures ANOVA (ANOVA for correlated samples) in combination with post hoc analysis.

3 Results

3.1 Spatial velocity composition of the transcranial transmission

The three Cartesian components of the promontory velocity were measured in all five heads for each measurement condition, as defined in Fig. 3. In this section, we present data from the 3D motion components of the ipsi- and contralateral promontory during each stimulation condition. The BC actuator was attached via a 5-N steel band at the mastoid or via the BI300 or Attract ® at the BAHA location. A set of individual measurements and their average (geometric mean) for stimulation via the BI300, is shown in Fig. 5, where each motion component as well as their combination are represented as magnitude and phase, normalized by the stimulus signal. The general data trend, noise floor, and intersample variability for both ipsi and contralateral 3D motion data can be seen.

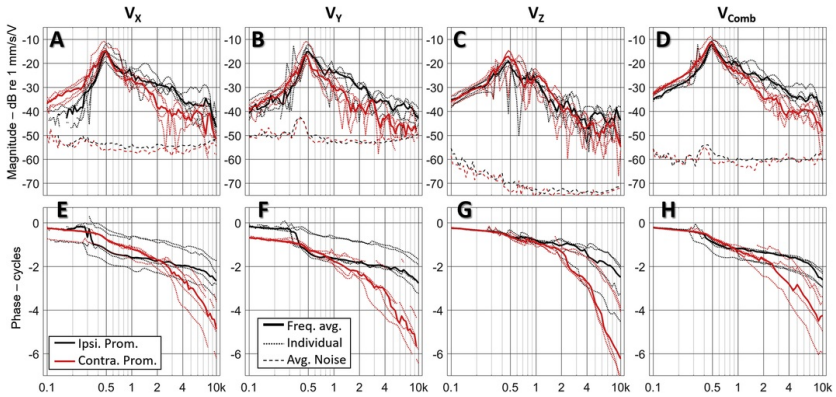

Fig. 5 Individual and averaged motion components of the ipsi- and contralateral promontory of five cadaver heads, stimulated via BI300 at the BAHA position. Each individual data point includes the 3 orthogonal motion components (A-C and E-F) and the corresponding combined motion (D and H), expressed as magnitude (A–D) and phase (E–H). Notes: Colors correspond to promontory location. Bold solid lines are median, across heads, and thin dotted lines are individual head data. Thin dashed lines in A-D are the averaged noise floor for each measurement condition across heads. (For interpretation of the references to color in this figure legend, the reader is referred to the Web version of this article.)

alt-text: Fig. 5

Fig. 5 A-C illustrate the magnitudes of the individual motion components, expressed for each individual head (n = 5) and their average. While the data indicated large intersample variability (±10 dB), particularly for higher frequencies, there were differences in the contribution of each motion component for ipsi- and contralateral promontories that were consistent across samples. Qualitatively similar trends across all samples were also seen in the phase of the individual motion components, as shown in Fig. 5 E-G. There was a general trend of increasing phase delay between the two sides with increasing frequency for all motion components. The intersample variability in the combined motion was smaller (±5 dB) overall with a more consistent trend (fewer local peaks and notches) in the individual and averaged responses for both promontories. Most of the data for the individual motion components were above the noise floor, the average of which is indicated as dashed lines in Fig. 5 A-C. Individual or averaged data with poor SNR (SNR =< 0 dB, relative to 2 SD above mean noise level) are removed from all plots. Gaps in the data occurred mostly for the low frequencies (below 250 Hz) because of the elimination of measurements that did not exceed the SNR criteria. Variations in the noise floor between individual motion components are discussed in Section 4.2.

Data in Fig. 5 were further processed and analyzed in order to quantitatively evaluate trends as well as to estimate the statistical significance of any observed differences between ipsi- and contralateral motion. Specifically, the data, composed of individual responses and per-frequency averages across heads, were separated into 5 frequency bands, as explained in Section 2.5. Results are shown in Fig. 6 A-H. In addition, the magnitude of each motion component, for each promontory, were normalized by the corresponding combined motion, resulting in a metric for the individual contribution of each component, shown in Fig. 6 I-K.

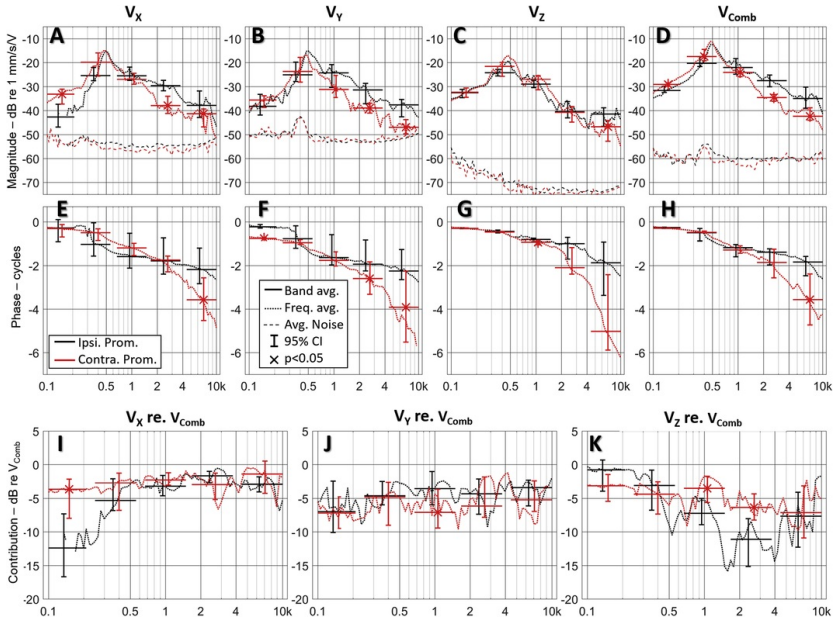

Fig. 6 Statistical analyses of the 3D component of the ipsi- and contralateral promontory motion of five cadaver heads, stimulated via BI300 at the BAHA position, as well as the relative contribution from each motion component. Each individual data point includes the 3 orthogonal motion components (A-C and E-F) and the corresponding combined motion (D and H), expressed as magnitude (A–D) and phase (E–H). Bottom row (I–J) is the contribution of each orthogonal component, relative to the corresponding combined motion. Notes: Colors correspond to promontory location (i.e., ipsi- and contra-). Dotted lines are median, across heads. Thin dashed lines in A-D are the averaged noise floor for each measurement condition across heads. (For interpretation of the references to color in this figure legend, the reader is referred to the We version of this article.)

alt-text: Fig. 6

Magnitude data of the X-component (along the anterior-posterior axis, Fig. 6A) of the contralateral promontory motion indicate on average 7 dB (95% confidence interval of 3–13 dB) greater motion below 300 Hz relative to the ipsilateral motion, indicative of a transcranial gain (i.e., negative transcranial attenuation). In contrast, the X-component of the contralateral promontory motion was an average of 5 dB (range = 2–10 dB) less motion above 1.5 kHz relative to the ipsilateral motion, indicative of transcranial attenuation. The phase of the X-component (Fig. 6E) showed a trend for increasing transcranial delay with increasing frequency, with a statistically significant delay of 1.4 cycles (range = 0.2 to 3 cycles) above 4 kHz. The relative contribution of the X-component to the combined motion of the promontory (Fig. 6I) was on average 8 dB (range = 1.5–12 dB) higher on the contralateral side than the ipsilateral side below 300 Hz. However, there was no significant difference in the contribution of the X-component between the two sides for higher frequencies (>600 Hz), where the average contribution was in the range of 2–3 dB below the combined motion.

The Y-component (along the superior-inferior axis, Fig. 6B) of the contralateral promontory motion was not significantly different from the ipsilateral promontory motion for low frequencies; however, there was an average 2–8 dB (range = 1–12 dB) transcranial attenuation above 600 Hz. The phase of the Y-component (Fig. 6F) showed a trend for a transcranial delay with increasing frequency, with significant delay of 0.7 cycles (range = 0.1 to 2 cycles) from 1.5 to 4 kHz and 1.6 cycles (range = 0.3 to 3.5 cycles) above 4 kHz. The relative contribution of the Y-component (Fig. 6J) did not show any significant difference or trend between the two sides for most of the frequency bands. The exception was the 0.6–1.5 kHz band, where the Y-component showed an average 3 dB (range = 1–6 dB) lower contribution of the contralateral side. Overall, the Y component for both sides contributed 3–7 dB less than the combined motion.

The Z-component (along the ear canal, Fig. 6C) of the contralateral promontory motion did not show significant difference compared to the ipsilateral promontory for the low and mid frequencies; however, there was an average of 5 dB (range = 1–10 dB) transcranial attenuation for the high frequencies (above 4 kHz). The phase of the Z-component (Fig. 6G) showed a trend for a transcranial delay with increasing frequency but was not significant due to the large intersample variation. The relative contribution of the Z-component to the combined motion (Fig. 6K) did not show any significant difference between the two sides except for the 0.6–4 kHz band, where there was a 0–9 dB higher contribution for the contralateral side. Within 0.1–4 kHz, there was an overall trend on both sides for decreasing contribution of the Z-component with increasing frequency, which appeared to disappear at higher frequencies.

The combined motion (Fig. 6D) showed smaller (+/−2-3 dB versus ± 5-7 dB) confidence intervals for all frequency bands relative to the individual components, which was indicative of smaller intersample variation based on this metric. The combined motion of the contralateral promontory indicated 1.5–4.5 dB transcranial gain below 600 Hz, and 1–12 dB transcranial attenuation at higher frequencies. The phase of the combined motion (Fig. 6D) showed a trend for increasing transcranial delay with frequency, with a significant delay of 1.5 cycles (range = 0.2 to 3 cycles) above 4 kHz.

3.2 Effect of coupling type on transcranial transmission

Data in Fig. 6, representing the BAHA stimulation location and BI300 coupling, were also obtained for the Attract® coupling and for 5-N steel band for mastoid stimulation. For each stimulation condition, the combined motion data (as in Fig. 6 D and H) at the contralateral promontory was normalized to the corresponding motion of the ipsilateral promontory. These data are shown in Fig. 7.

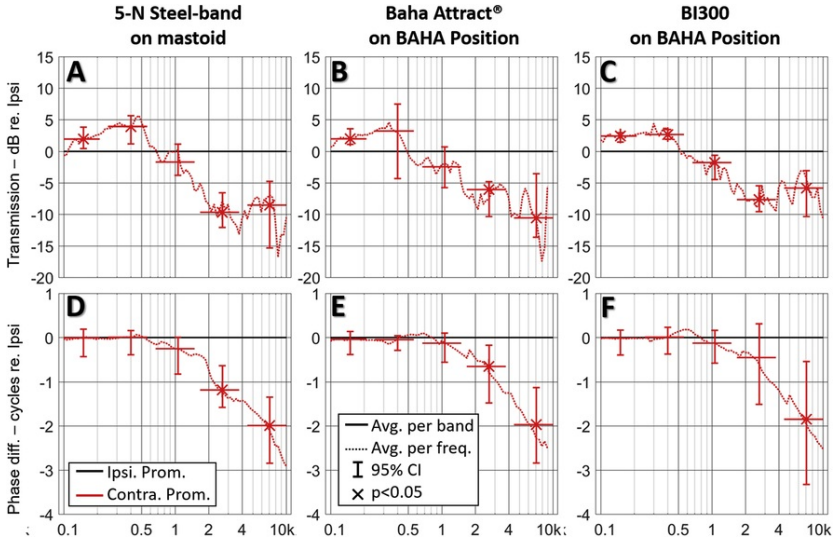

Fig. 7 The averaged combined motion of contralateral promontory motion relative to the ipsilateral promontory motion of five cadaver heads. Stimulation was applied via 5-N steel band (A, D) on the mastoid, Baha Attract (B, E), and BI300 (C, F) at the BAHA position. The magnitude is displayed in the top row (A–C), the phase in the bottom row (D–E). Notes: Colors correspond to promontory location (i.e., ipsi- and contra-). Dotted lines are median, across heads. (For interpretation of the references to color in this figure legend, the reader is referred to the Web version of this article.)

alt-text: Fig. 7

All coupling types yielded a significant transcranial gain in the range of 0.5–4.5 dB below 200 Hz. This was also found for the 300–600 Hz band but only for the steel band and BI300, with a gain of 1–5.5 dB. At mid to high frequencies (0.6–4 kHz), all coupling types showed a trend for increasing attenuation with increasing frequency, and the trend plateaued in the range of 3–15 dB above 4 kHz. In terms of transcranial phase delay, all coupling types showed a trend for increasing phase delay with increasing frequency above 500 Hz; however, the trend was significant only above 1.5 kHz for the steel band and the Attract ®, and only above 4 kHz for the BI300. Transcranial phase delay above 4 kHz was on average 2 cycles (range = 0.7 to 3.1 cycles) for all coupling types, with no significant difference between types.

3.3 Effect of varying stimulation location on promontory motion and ICP

Simultaneous measurements of ICP in the central CSF area (Fig. 2, location 1) and the ipsilateral promontory were conducted for several stimulation locations, while the coupling type was kept constant as a 5-N steel band. Stimulation locations included the forehead, neck, eye and ipsilateral mastoid, as defined in Fig. 2 and Section 2.1. This section contains an overview of the resultant velocity and pressure data, as well as their ratio. Stimulation at the ipsilateral mastoid was used as a reference in evaluation of the effect of the other simulation locations.

Fig. 8 displays results of the comparison between the stimulation locations based on the magnitude and phase of the combined motion of the ipsilateral promontory. Stimulation at the forehead (Fig. 8A) shows no significant difference relative to that at the mastoid below 600 Hz. At mid and high frequencies, the forehead stimulation showed a trend of lower promontory motion relative to mastoid stimulation, with an average 10 dB significant reduction (range = 4–15 dB) at 1.5–4 kHz, and 13 dB (range = 2–21 dB) at 4–10 kHz. Stimulation on the neck (Fig. 8B) performed similarly to the forehead stimulation at high frequencies, with a significant reduction in promontory motion of 19 dB

(range = 8–30 dB) at 4–10 kHz, relative to mastoid stimulation. However, unlike the forehead stimulation, neck stimulation resulted in 1–22 dB lower promontory motion below 1.5 kHz, relative to mastoid stimulation. The promontory motion for stimulation at the eye (Fig. 8C) followed a trend similar to neck stimulation, where there was a significant reduction at both high and low frequencies. The difference between the two was that there was a greater reduction in promontory motion, of 25 dB (range = 21–31 dB) at 4–10 kHz.

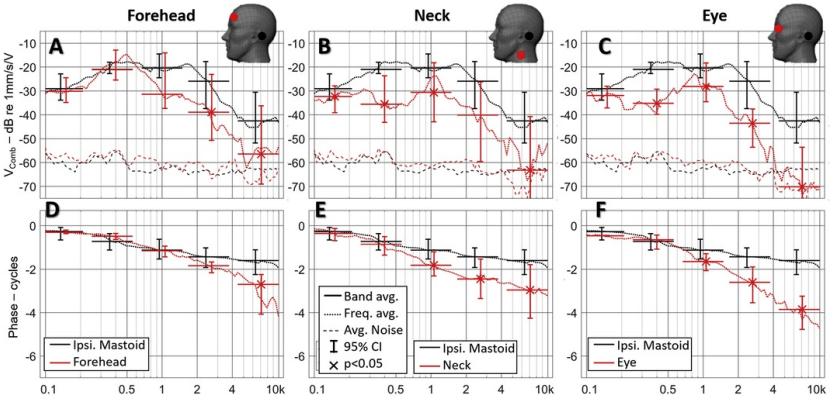

Fig. 8 Promontory motion, expressed as magnitude and phase of combined velocity (V_{Comb}), with varying stimulation position for coupling via a 5-N steel headband: (A, D) forehead vs. ipsilateral mastoid; (B,E) neck vs. ipsilateral mastoid, (C, F) eye vs. ipsilateral mastoid. Notes: Colors correspond to stimulation location. Dotted lines are median, across heads. Thin dashed lines in A-C are the averaged noise floor for each measurement condition, across heads. (For interpretation of the references to color in this figure legend, the reader is referred to the Web version of this article.)

alt-text: Fig. 8

The phase of the promontory motion followed a qualitatively similar pattern as the magnitude, where there was a general trend of faster accumulating phase delay with frequency for forehead, neck, and eye relative to mastoid stimulation. The trend was stronger for the softer stimulation areas, particularly for higher frequencies -- a phase delay of 1 cycle (range = 0.1 to 2.8 cycles) for forehead stimulation, 1.3 cycles (range = 0.5 to 2.5 cycles) for neck stimulation, and 2 cycles (range = 1.4 to 3.3 cycles) for eye stimulation.

Fig. 9 displays the ICP data from the central CSF region, which corresponds to the velocity data in Fig. 8. The ICP due to stimulation at the forehead (Fig. 9A) shows no significant difference relative to measurements for stimulation at the mastoid below 1.5 kHz and a trend for higher ICP at higher frequencies. In particular, there was a significant increase of 9 dB (range = 5–12 dB) from 1.5 to 4 kHz and of 11 dB (range = 1–17 dB) from 4 to 10 kHz. Stimulation on the neck (Fig. 9B) did not produce significantly different ICP relative to mastoid stimulation. However, there was a trend ($p = 0.07$) for a lower ICP at 300–500 Hz, which is qualitatively similar to the corresponding promontory motion decrease (Fig. 8B) in the same frequency range. Similarly, the eye stimulation (Fig. 9C) did not produce significantly different ICP relative to mastoid stimulation for most of the considered frequencies. The exception was the 300–500 Hz band, where the eye stimulation produced 2–19 dB lower ICP relative to the mastoid stimulation, which is also qualitatively similar to the corresponding promontory motion change (Fig. 8C) in the same frequency range.

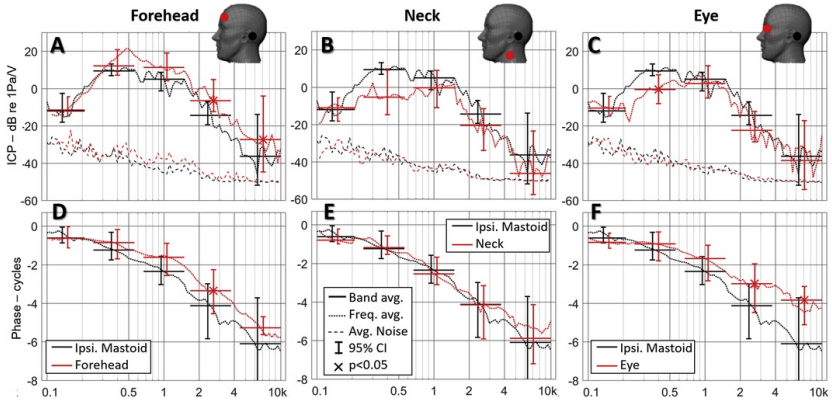

Fig. 9 Intracranial pressure (ICP), expressed as magnitude and phase, with varying stimulation position for coupling via a 5-N steel headband: (A, D) forehead vs. ipsilateral mastoid; (B, E) neck vs. ipsilateral mastoid, (C, F) eye vs. ipsilateral mastoid. Notes: Colors correspond to stimulation location. Dotted lines are median, across heads. Thin dashed lines in A-C are the averaged noise floor, across heads, for each measurement condition. (For interpretation of the references to color in this figure legend, the reader is referred to the Web version of this article.)

alt-text: Fig. 9

At most frequencies, there was a trend for the forehead stimulation (Fig. 9 D) to result in a shorter phase delay (~0.8 cycles) at higher frequencies compared to mastoid stimulation; however, this trend was significant only at 1.5–4 kHz. This was in contrast to the corresponding promontory response (Fig. 8D), which showed a trend of longer phase delay with increasing frequency. Neck and mastoid stimulation (Fig. 9E) produced similar phase delays. Overall, eye stimulation (Fig. 9F) produced less ICP phase delay than mastoid stimulation, and this significant trend increased with frequency to an average of 2.3 cycles above 4 kHz.

Fig. 10 was generated from calculation of the complex ratio of the data in Fig. 9 relative to the data in Fig. 8. The purpose was to illustrate the differences in timing and the amount of activation of the non-osseous versus osseous contents of the skull. A higher magnitude of the ratio in Fig. 10 A-C would correspond to a higher ICP for a given promontory motion, or lower promontory motion for a given ICP. In Fig. 10 D-F, less phase delay (higher values on the vertical axis) would correspond to earlier activation of the central temporal region relative to activation of the promontory.

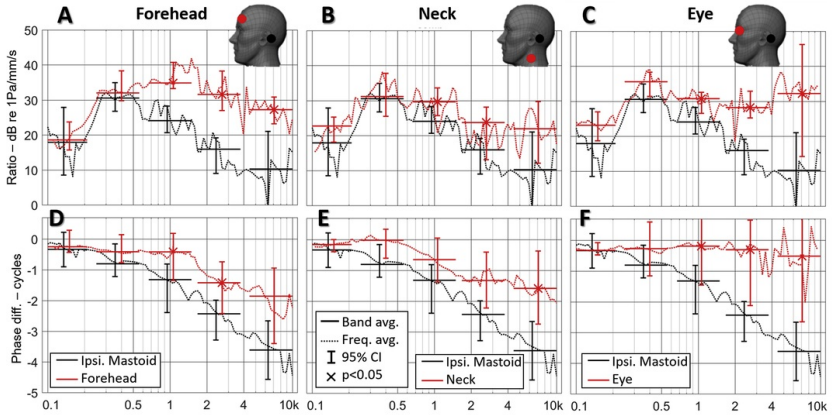

Fig. 10 Ratio of ICP in the central temporal region and the combined motion (V_{Comb}) of the ipsilateral promontory, expressed as magnitude and phase, with varying stimulation position for coupling via a 5-N steel headband: (A, D) forehead vs. ipsilateral mastoid; (B, E) neck vs. ipsilateral mastoid, (C, F) eye vs. ipsilateral mastoid. Notes: Colors correspond to stimulation location. Dotted lines are median, across heads. Thin dashed lines in A-C are the averaged noise floor, across heads, for each measurement condition. (For interpretation of the references to color in this figure legend, the reader is referred to the Web version of this article.)

alt-text: Fig. 10

Below 600 Hz, stimulation of the forehead (Fig. 10A) yielded a ratio that was not significantly different from the one for mastoid stimulation. However, at higher frequencies, there was a 9–16 dB higher ratio for 0.7–1.5 kHz, and 7–31 dB higher ratio from 4 to 10 kHz. When compared to the corresponding velocity (Fig. 8A) and ICP data (Fig. 9A) it can be seen that the increase of the ratio at higher frequencies is the combined result of a decrease in velocity and an increase in ICP.

Stimulation at the neck or eye (Fig. 10B and C) had a qualitatively similar effect on the ratio as the forehead stimulation, all relative to mastoid stimulation. Below 600 Hz, both neck and eye stimulation showed no significant difference to mastoid stimulation, based on the ICP to velocity ratio. At higher frequencies, both stimulation locations resulted in significantly higher ratios, in the range of 2–11 dB for the neck stimulation and 8–35 dB for eye stimulation. When compared to the corresponding velocity (Fig. 8B and C) and ICP data (Fig. 9B and C), it can be seen that the ratio increase for neck and eye stimulation is mainly due to a decrease in the corresponding promontory motion rather than a change in the ICP.

The phase difference between the ICP and promontory motion (Fig. 10D–F), indicated a consistent trend of smaller phase delay for stimulation on the forehead, neck and eye relative to the mastoid. This corresponds to an earlier activation of the CSF, relative to the promontory motion, at higher frequencies. The trend was most robust for non-osseous stimulation locations. In particular, above 4 kHz, the average phase delay decrease, relative to mastoid stimulation, was 1.7 cycles for forehead stimulation, 2.4 cycles for neck stimulation, and 2.9 cycles for eye stimulation.

3.4 ICP distribution

The ICP measurements were conducted at several regions within the skull cavity, as defined in Fig. 2 and Section 2.1, while simultaneously measuring the ipsilateral promontory motion. Measurements were repeated for each of three coupling conditions: 5-N steel band at the mastoid, Attract, and BI300 at the BAHA position. All ICP data were normalized by the corresponding motion data for the ipsilateral promontory in an equivalent way to the data shown in Fig. 10. The aim of the normalization was to illustrate ICP differences between coupling conditions, regardless of the absolute value of the corresponding promontory motion. The spatial distribution of the ICP within the skull and its timing relative to the promontory motion for each coupling type are described.

Fig. 11 displays data for a comparison of the magnitude and phase of the normalized ICP of the ipsilateral, contralateral, and central regions for each coupling condition. The 5-N steel band coupling produced a normalized ICP at the contralateral region (blue line in Fig. 11A) that was similar in magnitude (no significant difference) to the ipsilateral region, with the exception of the 4–10 kHz region, where the contralateral measurements had a 5.5 dB (range = 0.5–11 dB) lower response than the ipsilateral region. In contrast, the central region showed a significantly lower response at all frequencies, relative to the ipsilateral region. In particular, the response was reduced on average by 9 dB (range = 0.5–20 dB) below 600 Hz and 13 dB (range = 3–24 dB) above 1.5 kHz. The magnitudes of the normalized ICP for the Attract and BI300 coupling types (Fig. 11B and C) were similar to the contralateral and central regions, relative to the ipsilateral side. For both coupling conditions at the BAHA position, the response at the central location was consistently lower than at the ipsi or contralateral regions, with approximately 8.5–18 dB reduction on average across all frequencies. For both the Attract and the BI300 coupling types, the contralateral region showed no significant difference in normalized ICP magnitude from the ipsilateral region. Overall, there was a trend for a difference in the normalized ICP with respect to coupling type above 500 Hz at the ipsilateral and contralateral regions. Specifically, at 4–10 kHz, the steel band coupling produced on average 3–10 dB lower normalized ICP at the ipsi- and contralateral regions, compared to the Attract coupling type. In contrast, the normalized ICP at the central region was approximately the same for all coupling types, at 4–10 kHz.

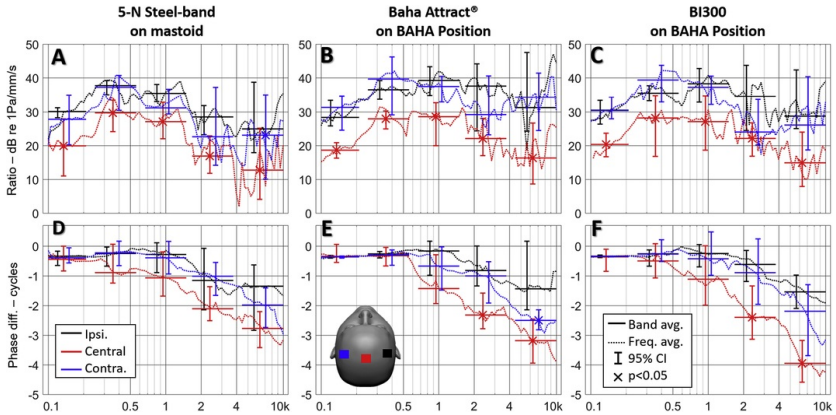

Fig. 11 Ratio of Intracranial pressure (ICP) versus promontory motion, expressed as magnitude and phase, for ipsilateral, contralateral and central regions of the cranial vault, with varying coupling type: (A, D) 5-N steel band on ipsilateral mastoid; (B, E); Attract on BAHA position; (C, F) BI300 on BAHA position. Notes: Colors correspond to hydrophone measurement location, while maintaining the same position at the promontory for 3D LDV measurements. Dotted lines are median, across heads. (For interpretation of the references to color in this figure

legend, the reader is referred to the Web version of this article.)

alt-text: Fig. 11

All coupling types showed a trend of increasing phase delay (Fig. 11D–F) at the central and contralateral regions, relative to the ipsilateral region, with increasing frequency. The phase delay at the central region was significantly different from the ipsilateral region above 1.5 kHz for the Attract and the BI300 coupling types. The difference relative to the ipsilateral region was approximately 1.1–1.8 cycles at 1.5–4 kHz and 1.7 to 2.4 cycles above 4 kHz. The phase delay at the contralateral region was significantly different from the ipsilateral region above 4 kHz for the BI300 coupling type only, with a difference of 0.4–2.6 cycles (median of 1.1 cycles).

Fig. 12 displays data of the magnitude and phase of the normalized ICP of the ipsilateral, anterior and posterior regions for each of the three coupling types. All coupling types showed a consistently lower normalized ICP (Fig. 12A–C) at the anterior region relative to the ipsilateral region, with a significant difference of 9–16 dB at 4–10 kHz. Coupling via Attract and BI300 resulted in significantly lower normalized ICP in the posterior region relative to the ipsilateral region, with a difference of 6–10 dB at 0.6–1.5 kHz. At frequencies below 600 Hz, the magnitude of the normalized ICP showed no significant differences between measurement locations or coupling types.

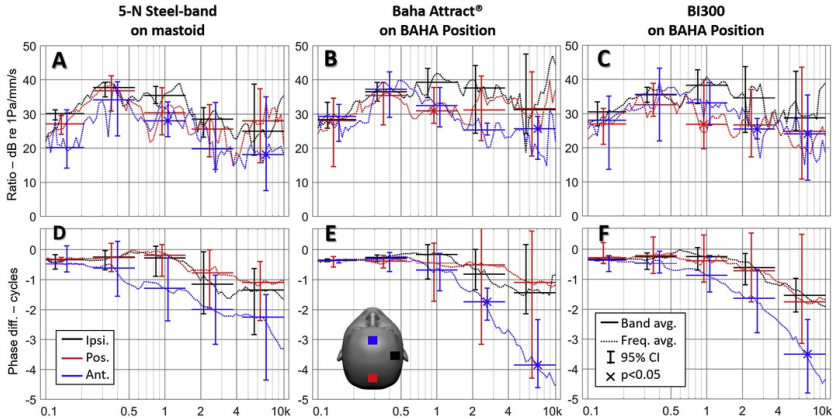

Fig. 12 Ratio of Intracranial pressure (ICP) versus promontory motion, expressed as magnitude and phase, for ipsilateral, posterior and anterior regions of the cranial vault, with varying coupling type: (A, D) 5-N steel band on ipsilateral mastoid; (B, E) Attract on BAHA position; (C, F) BI300 on BAHA position. Notes: Colors correspond to hydrophone measurement location, while maintaining the same position at the promontory for 3D LDV measurements. Dotted lines are median, across heads. (For interpretation of the references to color in this figure legend, the reader is referred to the Web version of this article.)

alt-text: Fig. 12

All coupling types showed a trend of increasing phase delay (Fig. 12D–F) at the anterior region (range = 1.9 to 2.4 cycles) relative to the posterior or the ipsilateral regions. This trend was significant only for the Attract and BI300 coupling types and only at frequencies above 1.5–4 kHz. In contrast, there was no significant difference in the phase delay between the posterior and ipsilateral regions, regardless of coupling type or stimulation frequency.

For each coupling type, the stimulation was kept constant between ICP measurements; therefore, the velocity response was approximately the same, with the exception of random or time dependent variations that were unavoidable with the current measurement procedure. The variation in the promontory response was quantitatively estimated based on comparisons between the consecutive velocity measurements, as shown in Fig. 13. The variation in the combined motion (Fig. 13D–F) for all coupling conditions was on the order of 1–3 dB across all frequencies and is discussed in detail in Section 4.1.

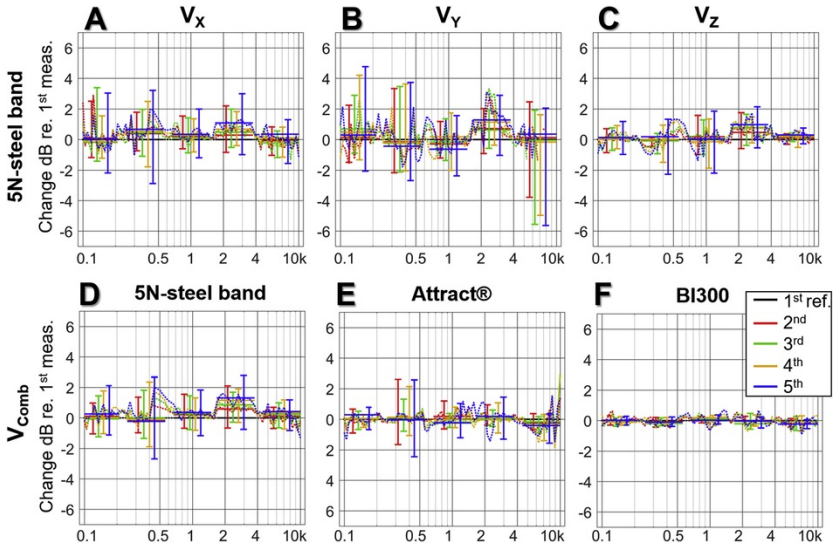

Fig. 13 Temporal drift of promontory velocity measurements, within a 1–3 h window across five heads. Subfigures (A–B) correspond to change in the individual motion components for stimulation via 5-N steel band. Subfigures D-F correspond to change in the combined motion for stimulation via 5-N steel band, Attract ®, and BI300 implant screw, respectively. Colors correspond to consecutive measurements, done at different hydrophone positions, while maintaining the 3D LDV position at the promontory. (For interpretation of the references to color in this figure legend, the reader is referred to the Web version of this article.)

alt-text: Fig. 13

4 Discussion

4.1 Considerations on methodology

4.1.1 Choice of samples and their temporal stability

Thiel embalmed heads were used because a full set of measurements for each head took 1–2 weeks. This would have been too long to assume sufficiently consistent material properties of the soft tissues if fresh heads were used. Previous work (Guignard et al., 2013) on Thiel-preserved temporal bones, has indicated that long-term (4–16 weeks) variation in promontory motion and skull response is approximately 3–5 dB on average across 0.1–10 kHz and up to 3–7 dB at 3–8 kHz, while short-term repeatability (e.g., 2 h) is approximately 1–2 dB for all frequencies. Based on these temporal drift estimates (each based on less than 4 samples) the test schedule for this study was organized such that the measurement time per measurement condition was reduced. For example, measurements of variation of stimulation position or transcranial attenuation were done together within 1 day. For this reason, it is assumed that for tests on position variation and transcranial attenuation, differences of less than 2–3 dB should be considered with caution even if they were estimated to be statistically significant.

We are not aware of any systematic investigation regarding potential changes in the acoustic response of the CSF/brain after Thiel embalming; however, this is known to be a general methodological limitation for acoustic research. An estimate of potential changes could be made based on reported changes in the middle ear response (Stieger et al., 2012), and specifically changes in the motion of the round window (RW) following air-conduction stimulation, which is likely to be conceptually similar (in terms to sensitivity to changes due to the preservation) to the CSF-dura interface in the cranial vault. It has been reported that there could be a 5–15 dB increase in the mid-frequency response of the RW in a Thiel preserved versus a fresh cadaver head. It should be noted that “normal” RW motion estimates vary between studies on the order of 10 dB or more at mid and high frequencies, where the RW motion becomes spatially complex (Sim et al., 2012; Stenfelt et al., 2004a,b (Remove the "a,b" as there is only one reference from this author from that year used on this manuscript.)). Overall, this indicates that there could be larger changes in the dynamic response of soft tissue (skin, dura, neck muscles, etc.), relative to skull bone, due to the Thiel embalming, however, the extend of these changes have not been evaluated.

In order to quantify the temporal drift of our measurements, we compared velocity measurements from the data set described in Section 3.4. In this set of experiments, only the ICP measurement location was varied, while the LDV measurement position remained at the ipsilateral promontory. This provided five consecutive velocity measurements under approximately the same conditions, one for each ICP measurement position, as shown in Figs. 10 and 11. Such a data set was available for all coupling conditions. The temporal drift in the promontory motion measurement for each head was defined as the ratio of the magnitude of promontory velocity for measurements 2–5 relative to measurement 1. The temporal drift was then averaged across

all heads and is presented in Fig. 13 in dB. Positive values indicate an increase in motion. The total time between the 1st and 5th measurement was between 1 and 3 h. Fig. 13 A-C display an overview of the temporal drift for the individual motion components at the ipsilateral promontory for mastoid stimulation via the steel band coupling. Fig. 13 D-E display an overview of the temporal drift of the combined motion at the ipsilateral promontory for all coupling types (i.e., steel band at mastoid; Attract and BI300 at BAHA position). Temporal drift within any of the individual motion components (Fig. 13A–C), for 5-N steel band coupling, was between 1 and 6 dB, with more drift for the X and Y components (2–6 dB) compared to the Z-component (0.5–2 dB). This is consistent with the lower SNR of the X and Y components due to the higher noise floor, relative to the Z component, as seen in Fig. 5 and discussed in Section 4.2. In contrast, the drift in the corresponding combined motion (Fig. 13D) was 0.5–2.5 dB. A comparison of the temporal drift of the combined motion between coupling conditions (Fig. 13D–F), indicates that promontory motion had the lowest temporal drift for the BI300 coupling with an average of less than 0.5 dB. This is consistent with our practical experience of using the different attachment types, where the 5-N steel band could allow for gradual sliding of the actuator away from the original attachment point, while the BI 300 provides a consistent connection.

4.1.2 Variability of promontory motion measurement

It has been shown previously that promontory motion can be used as an acceptable estimator of BC hearing sensation (Stenfelt and Goode, 2005a; Eeg-Olofsson et al., 2008, 2013; Dobrev and Sim, 2018; Stenfelt et al., 2004a,b), specifically at frequencies above the first resonance frequencies of the skull (i.e., 0.8–1 kHz) (Eeg-Olofsson et al., 2013). In order to estimate the potential hearing sensation due to osseous activation of the cochlea for any of the measurement conditions, promontory motion was measured at a location close to the round window. Previous studies have shown no significant dependence of promontory motion on the measurement location near the cochlea, based on comparisons of motions of the promontory and the otic capsule of the lateral semicircular canal in patients (Eeg-Olofsson et al., 2013).

During preliminary tests, an estimate was made of the dependence of the promontory measurements on variations in the measurement location between heads and experimental sessions. It was found that most of the detectable (>0.5–1 dB) variations in the velocity measurements at the promontory could be reduced by careful treatment of the bony surface at the measurement area. This included removing all soft tissue and moisture from the surface before applying (i.e., gluing) the retro-reflector medium. Without such treatment, various measurement artifacts were encountered such as rapid random variations in the LDV signal level, which in turn deteriorated the SNR. The LDV signal from the retroreflectors was maintained in the range of 90–100% to maximize SNR for all motion components.

4.1.3 Differences in the SNR between individual motion components

Overall, the SNR of all promontory motion measurements deteriorated below 0.25 kHz. This could be explained by the decreased response of the promontory at low frequencies due to the higher mechanical impedance of the skull (Stenfelt and Goode, 2005b). In addition to the lower motion, the optical design of the 3D LDV system is constrained by a tradeoff between sensitivity to in-plane components and spatial constraints (clear optical path and working distance) for the experimental setup and the sample. This results in the X and Y components having a higher noise floor than the Z component, with an increase of 15–25 dB and 25–30 dB, respectively, as seen on Fig. 5 A-B. When data were missing, the combined velocity was calculated based on the available components only. This was done in order to approximate the trend of the data at the affected frequencies. Overall, missing data did not affect any of the observations in this work.

4.2 Combined motion as a metric for promontory response

Data in Fig. 5 show that overall, the individual orthogonal components of the promontory response contained notches (“anti-resonances,” as termed in Eeg-Olofsson et al., 2013), with a width of less than 1/3 octave and depth of 10–20 dB or more. The particular location of the notches varied between heads and measurement sides. Overall, such behavior has been consistently reported in the literature with single component motion measurements in both fresh cadaver heads (Stenfelt and Goode, 2005b) and live humans (Eeg-Olofsson et al., 2013, Fig. 2 in particular). This could contribute to higher apparent sample variability, resulting in the need for measurements on more samples in order to reach statistically significant conclusions.

Fig. 6 I

-K suggest that all motion components contribute comparably to the combined motion, with magnitudes of 2–7 dB less than the combined velocity, on average across all frequencies. However, the individual contributions have frequency dependence, with variations of more than 10–15 dB for specific frequency bands and between the two promontories. The Z component in particular, which is typically used in research, is 3–12 dB smaller than the combined motion above 500 Hz, and has on average up to a 5 dB higher contribution at the contralateral versus the ipsilateral promontory. This has been reported previously by Stenfelt and Goode (2005b). This suggests that using only one motion component (e.g., along the ear canal) to define cochlear motion could potentially lead to an under-estimation of the full motion of the cochlea and an overestimation of the transcranial attenuation. In addition, 3D motion could also be a better descriptor of BC hearing thresholds in audiometric tests (Stenfelt, 2012; Stenfelt et al., 2004a,b), (remove "a,b")as has been shown in comparisons (Dobrev and Sim, 2018) of transcranial attenuation based on combined motion and data in patients (Ito et al., 2011).

4.3 Transcranial attenuation

4.3.1 Velocity composition of the transcranial attenuation and delay

As displayed in Fig. 6 A-D, the measurements of the ipsi- and contralateral promontory motion magnitude for stimulation via BI300 indicate a significant transcranial attenuation across all motion axes as well as the combined motion at mid and high frequencies. However, the amount of attenuation varies with frequency and spatial direction. For example, while the combined motion indicated a significant attenuation above 600 Hz, other axes reached significant attenuation only at higher frequencies, mainly due to larger intersample variability. In contrast to the mid- and high frequencies, at low frequencies (below 300 Hz), the motion difference between the ipsi- and contralateral promontories followed a trend of negative attenuation (transcranial gain) in all motion directions as well as the combined motion. This behavior was significant in the combined motion data with a median gain of 2–3 dB at 100–600 Hz, and it was mainly due to the X-component (along the anterior-posterior direction) with a median gain of 7 dB.

Data (Fig. 6I–K) from the contribution of each motion component indicate significant differences between the spatial composition of the ipsi- and contralateral motion, suggestive of not only transcranial transmission (attenuation or gain) but also change in the main direction of motion, potentially resulting in differences in the significance of the contribution of each BC pathway (e.g., contribution of middle ear, inertia, otic capsule deformation) to the activation of the contralateral cochlea (Stenfelt and Goode, 2005a). Differences in the spatial composition of the ipsi- and contralateral promontory motion have been reported previously (Dobrev and Sim, 2018; Stenfelt and Goode, 2005b). On average, there is less difference between motion components at the contralateral side than at the ipsilateral side, which supports data by Stenfelt and Goode (2005b). This suggests that transcranial transmission reduces any directionality (predominance of one component) regardless of the motion composition of the ipsilateral side. It could then be hypothesized that when using a BCHA for treatment of single sided deafness, the directionality (motion composition) of the contralateral stimulation would not be critical for efficient transcranial transmission. This potentially allows for new BCHA actuator designs that do not have to vibrate predominantly along the normal to the skull surface (out-of-plane) when transmitting mid and high frequencies (above 1 kHz). Without such design constraints, new actuator designs could have reduced overall thickness (protrusion away from the skull) for better aesthetics and simpler installation, which is particularly important for implanted actuators. For example, thin flat (or curved) actuators could be embedded in the thin (1–2 mm) top layer of the skull bone and be used to compress the skull's surface tangentially (in-plane compression) instead of normally (out-of-plane bending).

The phase of all individual motion components and the combined motion showed a consistent trend of increasing transcranial phase delay with increasing frequency. The maximum phase delay was on average 1.7 to 2.2 cycles for all motion components. There was a general trend for the Z-component to have the largest phase delay and the X-component the smallest, but this could not be significant statistically due to the large intersample variability in the phase at high frequencies. This could be an indication of a different transmission mode for each stimulation direction, thus potentially affecting the perceived transcranial delay.

4.3.2 Dependence on coupling type

All coupling types resulted in qualitatively similar behavior of transcranial attenuation and delay, as shown in Fig. 7. It should be noted that stimulation location for the steel band coupling was different (mastoid) from that for the Attract and BI300 (BAHA location). For all coupling types, there was a transcranial attenuation of 6–10 dB above 1 kHz, similar to results reported in the literature (Nolan and Lyon, 1981, Håkansson et al., 1986; Stenfelt, 2012). There was a trend for lower attenuation for BI300 coupling compared to the other coupling types at the highest frequencies (above 4 kHz), but this trend was not statistically significant. However, Stenfelt and Goode (2005b), in their work with fresh cadaver heads, have shown a similar trend above 4 kHz with a connection based on a M3 screw (approximately similar to BI300). Such observations were qualitatively confirmed in live human subjects by Stenfelt (2012), through direct comparison of transcranial attenuations for stimulation at the BAHA position via a BI300 versus stimulation at the mastoid via a steel band. This suggests that the observed trend in the magnitude displayed in Fig. 6 A-C might be due to a combination of stronger transcranial attenuation at the mastoid location and the more efficient coupling provided by the BI300. It could then be hypothesized that direct bone coupling (BI300 or implanting of the actuator) located closer to the cochlea, such as in the case of some newly developed BCHA actuators (Håkansson et al., 2010; Dobrev et al., 2018b), would provide better selectivity for stimulation of the ipsilateral relative to the contralateral cochlea.

All coupling types showed a significant transcranial gain (i.e., negative attenuation) of approximately 2–5 dB, based on the combined motion. Such a transcranial gain has also been observed in previous research with 1D and 3D velocity measurement in cadaver heads (Stenfelt and Goode, 2005b; Dobrev and Sim, 2018; Dobrev et al., 2018b) and in 1D velocity measurements in patients (Stenfelt, 2012; Eeg-Olofsson et al., 2011a, 2011b). A hypothesis for its occurrence is based on a rigid-body-like motion of the head at low frequencies, composed of a translation (approximately along the stimulation direction) and rotation (particularly around the superior-inferior axis) components. Such motion combination could result in higher tangential velocity (relative to the axis of rotation) for the contralateral side. Since both promontories have the same translation velocity due to the rigid body motion, there could a higher combined motion at the contralateral cochlea (Dobrev and Sim, 2018).

4.4 Effect of stimulation location on the osseous and non-osseous response

Measurements reported in Section 3.3 are a continuation of previous work (Röösli et al., 2016) from our research group but using improved measurement methodology including measurements of all motion components (Dobrev and Sim, 2018) as well as measurement of the phase for both motion and ICP. The ipsilateral promontory motion data from the current measurement set (Fig. 8) indicates both frequency and stimulation location dependence. All stimulation locations result in similar (within <5 dB on average) promontory motion at low frequencies (below 300 Hz) with no significant phase differences, potentially due to the rigid-body-like motion of the head at low frequencies. Above 300 Hz, all stimulation locations away from the mastoid produce a lower response of the promontory, and the trend increases with frequency. This trend is stronger for stimulation on non-osseous locations (i.e., neck and eye) versus the osseous locations (i.e., forehead), as has been observed previously by Röösli et al. (2016). This could be due to the combined effect of distance between the stimulation location and the cochlea, and the different mechanical point impedances at each stimulation location (Stenfelt and Goode, 2005b). In addition, there could be differences in the behavior of the actuator when coupled to the eye, since this was not explored in our study.

There were some qualitative differences in the motion data of our study relative to results from Röösli et al. (2016). In particular, the forehead stimulation produced significantly lower promontory motion at high frequencies (above 4 kHz) with an average of 13 dB below the motion due to mastoid stimulation, similar to audiometric measurements (Reinfeldt et al., 2013). In Röösli et al. (2016), the forehead stimulation produced similar or even higher promontory motion, with an average of 1–2 dB above the motion due to mastoid stimulation. One methodological difference between the two sets of measurements was the positioning of the head. For the study by Röösli et al. (2016), the head was placed on its face in a rubber ring; whereas, we supported the head on the neck. Even so, it is unclear how this difference in position may have affected promontory motion at higher frequencies.

The phase data (Fig. 8D–F) show a general trend of increasing phase delay with increasing frequency for all stimulation locations relative to the mastoid; however, the phase delay is larger at higher frequencies for non-osseous (eye) versus osseous (forehead) stimulation locations. This could be due to a combination of different material properties (different frequency dependencies) at the stimulation location (Håkansson et al., 2008) as well as potential differences between the different propagation pathways from each stimulation location to the cochlea (Stenfelt and Goode, 2005a; Dobrev et al., 2016; Röösli et al., 2016). It should be noted that since the effect of the neck or eye coupling to the output of the actuator is unknown, this could be affecting the results as well.

The ICP data in the central CSF region, shown in Fig. 9, indicate both frequency and stimulation location dependence; however, the data do not indicate dependence on the distance between the stimulation location and the pressure measurement region in the center of the skull cavity. This is clearly visible when comparing forehead and mastoid stimulation (Fig. 9A), where the approximate distance from the two stimulation locations and the hydrophone is similar (6–7 cm for both). In this case, the forehead stimulation produces consistently higher ICP than the mastoid stimulation for all frequencies above 300 Hz, and the difference tends to increase with frequency, reaching an average significant difference of 9 dB above 4 kHz. This could be explained by the lower mechanical impedance at the forehead relative to the skull (Stenfelt and Goode, 2005b), giving rise to a higher velocity of the surrounding skull bone in the vicinity of the stimulation location, which in turns produces higher pressures at the bone-CSF interface. The phase data of the ICP suggest lower phase delays for stimulation at the forehead; however, the trend does not show the significant change with increasing frequency that occurred with the ICP magnitude, but rather a constant offset of approximately 1 cycle.

Stimulation of non-osseous locations produces ICP similar (no significant difference) to mastoid stimulation at nearly all frequencies, also seen in Röösli et al. (2016) for stimulation at the forehead and eye. However, ICP with neck stimulation in Röösli et al. (2016) shows a much lower response than the mastoid stimulation, with an average difference of 15–25 dB above 1 kHz. The differences in the observed ICP behavior with neck stimulation could be due to methodological differences, such as neck stimulation location and the support arrangement for the cadaver head. The neck stimulation location was on the sternocleidomastoid muscle, around 5–7 cm below its insertion on the mastoid, which was closer to the ear canal than the stimulation location of 10–12 cm distance used in Röösli et al. (2016). The difference in stimulation location was due to the shorter available (accessible) neck area of the cadaver heads used in this study, which was caused by the vertical head support, in contrast to the fully exposed neck in Röösli et al. (2016). The head support setup in this study preloaded the neck with the weight of the head, which could have improved the soft-tissue coupling. In Röösli et al. (2016), the head was supported horizontally on its contralateral side via a silicone gel cushion, leaving the neck in a free (unloaded) state.

One general limitation of the promontory motion data described in Section 3.3 is that some of the motion data for the neck and eye stimulations was near or below the noise floor, especially for frequencies above 4 kHz. When measurements of some of the individual motion components (particularly the X and Y components) reached their corresponding noise floor (c.f., Section 4.1), the combined motion was calculated with only the remaining components. This resulted in an apparent decrease of the noise floor of the combined motion, as seen in the dashed red lines above 4 kHz in Fig. 8 B and C. This could have resulted in greater variability in the remaining data potentially affecting the median, regardless of the statistical significance. Thus, velocity data at those frequencies for neck and eye stimulation should be interpreted with caution. This could also be the cause of potential differences with Röösli et al. (2016), where there was also poor SNR at high frequencies for neck and eye stimulation.

For stimulation at the eye and neck, there is a trend for lower ICP (10 and 15 dB, respectively) relative to the mastoid stimulation, at 300–600 Hz; however, this coincides with a similar drop in the corresponding promontory velocity, which was also seen in Röösli et al. (2016). This is potentially due to a difference in the force output of the BC actuator at 300–600 Hz for the different coupling conditions rather than differences in the activation mechanisms of the ICP for non-osseous versus osseous stimulation.

There is no significant difference in the phase delay for stimulation on the neck and the mastoid. However, stimulation on the eye produces significantly lower phase delay at the central region of the CSF, with lower slope of phase delay, than for the mastoid stimulation, particularly above 1.5 kHz. This suggests a faster (less phase delay) pathway to the CSF from the eye, but it is not more efficient (similar magnitude) than for stimulation at the mastoid, as demonstrated previously (Sim et al., 2016; Röösli et al., 2016).

In order to illustrate the differences in the activation of the osseous and non-osseous contents due to different stimulation locations, the complex ratio of the ICP and the combined motion was calculated, as shown in Fig. 10. These data indicate significant increase in the magnitude and decrease in the phase of the ratio for all stimulation locations relative to the mastoid with a general trend of increase with increasing frequency. The largest differences were seen for stimulation at the eye, with an average increase of 23 dB above 4 kHz, which was more than for any other stimulation location. The phase of the complex ratio for eye stimulation was approximately constant with frequency, accumulating an average of 2.5 cycles of lead (less phase delay) relative to stimulation at the mastoid. It can be hypothesized that stimulation on the eye activates the CSF more efficiently than do the osseous sections of the skull (based on promontory motion only), potentially indicating a completely non-osseous pathway. This potential pathway could be passing via the CSF and exciting the cochlea fluid via a non-osseous “3rd window” path (e.g., auditory

nerve) rather than via deformations of the temporal bone at high frequencies (Sim et al., 2016; Röösli et al., 2016; Sohmer and Freeman, 2004; Freeman et al., 2000; Chordekar et al., 2012; Perez et al., 2011). Recently, potential direct evidence for such a non-osseous pathway from the CSF to the cochlea has been reported by measuring OAE elicited by direct dura stimulation in live human subjects intraoperatively (Stump et al., 2018). This potential pathway could be used for a new type of BCHA, similar in operation to underwater speakers. Such implantable devices could alleviate the need for minimal skull thickness in the area of implantation, as they could be in direct contact with the CSF or dura.

Below 300 Hz, there were no significant differences in the ICP, promontory motion or their ratio for all stimulation locations. This is consistent with the rigid-body-like behavior of the head. Since both the combined motion and the ICP are direction insensitive metrics (Dobrev and Sim, 2018), potential differences in the direction of the rigid body motion will not be detected by the current measurements.

4.5 Spatial distribution of ICP and dependence on coupling type

Comparison of the normalized ICP between the ipsi-, central and contralateral regions (Fig. 11) shows a consistent trend of similar responses for the ipsi- and contralateral regions but significantly lower response for the central region for all frequencies and coupling types. In particular, the phase of the normalized ICP showed a trend for longer phase delays at the central region relative to the ipsilateral side, with more significant and larger differences at higher frequencies. The contralateral region also showed a phase delay relative to the ipsilateral region; however, the average difference was smaller, compared to the central region. Since the contralateral region appears to have less delay and attenuation than the central region, sound energy should be flowing through the skull base or at the peripheral regions of the fluid, thus circumventing the central region.

Data in Fig. 12 help further discern the direction of sound energy flow, while circumventing the central CSF region. Comparison between subfigures D-F of Figs. 11 and 12, indicates that the longer phase delay of the center and the anterior are similar. There is also a general trend of lower magnitude at the anterior; however, the difference relative to the ipsilateral and posterior regions is only 5–7 dB on average and is significant only at higher frequencies. In contrast, the posterior is activated with no significant phase delay or attenuation relative to the ipsilateral region, regardless of coupling condition. This suggests that the posterior is activated sooner and with less attenuation than the anterior and almost simultaneously with the ipsilateral region.

Combining observations from all five stimulation locations (Figs. 11 and 12), one possible hypothesis is that propagation of vibrational energy from the ipsilateral side is passing first through the occipital and temporal sections of the skull (which are thicker), which activates the posterior and contralateral skull sections first and the anterior sections later. This in turn activates the fluid content of the skull cavity in the proximity of the skull bone. Sound energy from the skull-fluid boundary is then propagated, with transmission delay and attenuation, to the central and anterior regions. This hypothesis and corresponding data are in qualitative agreement with spatial pattern of power flow within the CSF, numerically simulated via the finite element model (FEM) LiUHead (Chang et al., 2018).

This general behavior is consistent across all coupling types; however, phase differences between the central and the peripheral regions are larger with coupling types that provide more direct osseous stimulation. In particular, for 4–10 kHz, the median phase delay of the normalized ICP between the central and ipsilateral regions is 0.8 cycles (not statistically significant) for the steel band, 1.7 cycles for Attract, and 2.4 cycles (or 0.4 ms at 6 kHz) for BI300. This suggests additional complexities in the propagation pattern potentially due to different activation mechanisms for each coupling type. Explanation of these phenomena could come through more detailed pressure and velocity measurements and comparisons with FEM (Chang et al., 2018).

We hypothesize that the intracranial pressure and skull vibration cannot be looked at individually as they always interact, at any frequency and stimulation type. Our study does not investigate this interaction, thus we cannot separate their individual contributions. However, we hypothesize, that our methodology could detect a change in the interaction of the osseous and non-osseous pathways for different stimulation types, particularly based on cahnges in the trends of the phase differences between the ICP and vibratory motion. In addition, the combination of all these data and observations could be used to verify and improve existing numerical models, which in turn could be used for the design of new BCHA as well as optimization of their placement, coupling and corresponding surgical procedure.

5 Conclusions

Comprehensive experiments, including simultaneous motion and pressure measurements, with various stimulation positions and coupling methods allow for detailed exploration and differentiation of the individual contributions of the various bone conduction pathways.

Utilization of combined 3D promontory motion gives more precise information on bone vibrations with lower intersample variability than any individual component. The 3D motion measurements indicate that the promontory undergoes spatially complex motion with similar contributions from all 3 orthogonal motion components, regardless of stimulation mode. Additionally, transcranial transmission changes not only the magnitude of the transmitted motion but also its spatial composition, such that the contralateral promontory motion does not follow the ipsilateral stimulation direction above 0.5 kHz. In addition, single axis motion measurements could be overestimating the transcranial attenuation below 0.5 kHz.

Comprehensive combination of motion and pressure measurements across the head, combined with variation of the stimulation condition, could reveal details about the acoustic power transmission within the skull. Preliminary

data indicate that sound energy is transmitted from the stimulation area to the posterior and contralateral sides via skull bone (potentially through the skull base) before activating the anterior parts and consequently the central region of the CSF.

Uncited References

Stenfelt and Håkansson, 1999; Vasavada et al., 2001.

Acknowledgeements (Ignore this change.)

Funding for this study was provided by a grant (SNF 325230-166377) from the Swiss National Science Foundation.

References

Adelman C., Fraenkel R., Kriksunov L. and Sohmer H., Interactions in the cochlea between air conduction and osseous and non-osseous bone conduction stimulation, *Eur. Arch. Oto-Rhino-Laryngol.* **269** (2), 2012, 425–429.

Barany E.A., A contribution to the physiology of bone conduction, *ActaOtolaryngol. Suppl.* **26**, 1938, 1–223.

von Békésy G., Zur Theorie des Hörens bei der Schallaufnahme durch Knochenleitung, *Ann. Phys.* **13**, 1932, 111–136.

Chang Y., Kim N. and Stenfelt S., Simulation of the power transmission of bone-conducted sound in a finite-element model of the human head, *Biomechanics Model. Mechanobiol.* 2018, 1–15.

Chordekar S., Kriksunov L., Kishon-Rabin L., Adelman C. and Sohmer H., Mutual cancellation between tones presented by air conduction, by bone conduction and by non-osseous (soft tissue) bone conduction, *Hear. Res.* **283** (1–2), 2012, 180–184.

Dobrev I. and Sim J.H., Magnitude and phase of three-dimensional (3D) velocity vector: application to measurement of cochlear promontory motion during bone conduction sound transmission, *Hear. Res.* **364**, 2018, 96–103, https://doi.org/10.1016/j.heares.2018.03.022.

Dobrev I., Sim J.H., Aqtashi B., Huber A.M., Linder T. and Röösli C., Effects of middle ear quasi-static stiffness on sound transmission quantified by a novel 3-axis optical force sensor, *Hear. Res.* **357**, 2018a, 1–9.

Dobrev I., Sim J.H., Pfiffner F., Huber A.M. and Röösli C., Performance evaluation of a novel piezoelectric subcutaneous bone conduction device, *Hear. Res.* 2018b.

Dobrev I., Sim J.H., Stenfelt S., Ihrle S., Gerig R., Pfiffner F., Eiber A., Huber A.M. and Röösli C., Sound wave propagation on the human skull surface with bone conduction stimulation, *Hear. Res.* **355**, 2017, 1–13.

Dobrev I., Stenfelt S., Röösli C., Bolt L., Pfiffner F., Gerig R., Huber A. and Sim J.H., Influence of stimulation position on the sensitivity for bone conduction hearing aids without skin penetration, *IJA (Int. J. Acarol.)* **55** (8), 2016 439–446.

Eeg-Olofsson M., Stenfelt S., Tjellström A. and Granström G., Transmission of bone-conducted sound in the human skull measured by cochlear vibrations, *Int. J. Audiol.* **47** (12), 2008, 761–769.

Eeg-Olofsson M., Stenfelt S., Håkansson B., Taghavi H., Reinfeldt S., Östli P. and Granström G., Optimal position of a new bone conduction implant, *Cochlear Implants Int.* **12** (Suppl. 1), 2011a, S136–S138.

Eeg-Olofsson M., Stenfelt S. and Granström G., Implications for contralateral bone-conducted transmission as measured by cochlear vibrations, *Otol. Neurotol.* **32** (2), 2011b, 192–198.

Eeg-Olofsson M., Stenfelt S., Taghavi H., Reinfeldt S., Håkansson B., Tengstrand T. and Finizia C., Transmission of bone conducted sound–correlation between hearing perception and cochlear vibration, *Hear. Res.* **306**, 2013, 11–20.

Freeman S., Sichel J.Y. and Sohmer H., Bone conduction experiments in animals–evidence for a non-osseous mechanism, *Hear. Res.* **146** (1–2), 2000, 72–80.

Guignard J., Stieger C., Kompis M., Caversaccio M. and Arnold A., Bone conduction in Thiel-embalmed cadaver heads, *Hear. Res.* **306**, 2013, 115–122.

Håkansson B., Carlsson P. and Tjellström A., The mechanical point impedance of the human head, with and without skin penetration, *J. Acoust. Soc. Am.* **80** (4), 1986, 1065–1075.

Håkansson B., Eeg-Olofsson M., Reinfeldt S., Stenfelt S. and Granström G., Percutaneous versus transcutaneous bone conduction implant system: a feasibility study on a cadaver head, *Otol. Neurotol.* **29** (8), 2008, 1132–1139

Håkansson B., Reinfeldt S., Eeg-Olofsson M., Östli P., Taghavi H., Adler J., Gabrielsson J., Stenfelt S. and Granström G., A novel bone conduction implant (BCI): engineering aspects and pre-clinical studies, *IJA (Int. J. Acarol.)* **49** (3), 2010, 203–215.

Hood J.D., The principles and practice of bone conduction audiometry: a review of the present position, *Laryngoscope* **70** (9), 1960, 1211–1228.

Hoyer H.E. and Dorheide J., A study of human head vibrations using time-averaged holography, *J. Neurosurg.* **58** (5), 1983, 729–733.

Hulecki L.R. and Small S.A., Behavioral bone-conduction thresholds for infants with normal hearing, *J. Am. Acad. Audiol.* **22** (2), 2011, 81–92.

Hurley R.M. and Berger K.W., Relationship between vibrator placement and bone conduction measurements with monaurally deaf subjects, *J. Aud. Res.* **10** (2), 1970, 147–150.

Ito T., Röösli C., Kim C.J., Sim J.H., Huber A.M. and Probst R., Bone conduction thresholds and skull vibration measured on the teeth during stimulation at different sites on the human head, *Audiol. Neurotol.* **16** (1), 2011, 12–22.

Lilliefors H.W., On the Kolmogorov-Smirnov test for normality with mean and variance unknown, *J. Am. Stat. Assoc.* **62** (318), 1967, 399–402.

McKnight C.L., Doman D.A., Brown J.A., Bance M. and Adamson R.B., Direct measurement of the wavelength of sound waves in the human skull, *J. Acoust. Soc. Am.* **133** (1), 2013, 136–145.

Nolan M. and Lyon D.J., Transcranial attenuation in bone conduction audiometry, *JLO* **95** (06), 1981, 597–608.

Perez R., Adelman C. and Sohmer H., Bone conduction activation through soft tissues following complete immobilization of the ossicular chain, stapes footplate and round window, *Hear. Res.* **280** (1–2), 2011, 82–85.

Pfiffner F., Caversaccio M.D. and Kompis M., Audiological results with Baha® in conductive and mixed hearing loss, In: *Implantable Bone Conduction Hearing Aids* **vol. 71**, 2011, Karger Publishers, 73–83.

Ravicz M.E., Melcher J.R. and Kiang N.Y.S., Acoustic noise during functional magnetic resonance imaging, *J. Acoust. Soc. Am.* **108** (4), 2000, 1683–1696.

Reinfeldt S., Stenfelt S., Good T. and Håkansson B., Examination of bone-conducted transmission from sound field excitation measured by thresholds, ear-canal sound pressure, and skull vibrations, *J. Acoust. Soc. Am.* **121** (3), 2007, 1576–1587.

Reinfeldt S., Stenfelt S. and Håkansson B., Estimation of bone conduction skull transmission by hearing thresholds and ear-canal sound pressure, *Hear. Res.* **299**, 2013, 19–28.

Röösli C., Dobrev I., Sim J.H., Gerig R., Pfiffner F., Stenfelt S. and Huber A.M., Intracranial pressure and promontory vibration with soft tissue stimulation in cadaveric human whole heads, *Otol. Neurotol.* **37** (9), 2016, e384–e390.

Sim J.H., Dobrev I., Gerig R., Pfiffner F., Stenfelt S., Huber A.M. and Röösli C., Interaction between osseous and non-osseous vibratory stimulation of the human cadaveric head, *Hear. Res.* **340**, 2016, 153–160.

Sim J.H., Chatzimichalis M., Röösli C., Laske R.D. and Huber A.M., Objective assessment of stapedotomy surgery from round window motion measurement, *Ear Hear.* **33** (5), 2012, e24–e31.

Snyder J.M., Interaural attenuation characteristics in audiometry, *Laryngoscope* **83** (11), 1973, 1847–1855.

Sohmer H., Freeman S., Geal-Dor M., Adelman C. and Savion I., Bone conduction experiments in humans - a fluid pathway from bone to ear, *Hear. Res.* **146**, 2000, 81–88.

Sohmer H. and Freeman S., Further evidence for a fluid pathway during bone conduction auditory stimulation, *Hear. Res.* **193**, 2004, 105–110.

Steiner L.A. and Andrews P.J.D., Monitoring the injured brain: ICP and CBF, *BJA: Br. J. Anaesth.* **97** (1), 2006, 26–38.

~~Stenfelt S.P. and Håkansson B.E., Sensitivity to bone-conducted sound: excitation of the mastoid vs the teeth, *Scand. Audiol.* **28** (3), 1999, 190–198.~~

Stenfelt S., Hato N. and Goode R.L., Fluid volume displacement at the oval and round windows with air and bone conduction stimulation, *J. Acoust. Soc. Am.* **115** (2), 2004a, 797–812.

Stenfelt S. and Goode R.L., Bone-conducted sound: physiological and clinical aspects, *Otol. Neurotol.* **26** (6), 2005a, 1245–1261.

Stenfelt S. and Goode R.L., Transmission properties of bone conducted sound: measurements in cadaver heads, *J. Acoust. Soc. Am.* **118** (4), 2005b, 2373–2391.

Stenfelt S., Simultaneous cancellation of air and bone conduction tones at two frequencies: extension of the famous experiment by von Békésy, *Hear. Res.* **225**, 2007, 105–116.

Stenfelt S., Transcranial attenuation of bone-conducted sound when stimulation is at the mastoid and at the bone conduction hearing aid position, *Otol. Neurotol.* **33** (2), 2012, 105–114.

Stenfelt S., Inner ear contribution to bone conduction hearing in the human, *Hear. Res.* **329**, 2015, 41–51.

Stenfelt S., Hato N. and Goode R.L., Fluid volume displacement at the oval and round windows with air and bone conduction stimulation, *J. Acoust. Soc. Am.* **115** (2), 2004b, 797–812. (This repeats with the Stenfelt 2004a - delete 2004b and change 2004a to just 2004.)

Stieger C., Candreia C., Kompis M., Herrmann G., Pfiffner F., Widmer D. and Arnold A., Laser Doppler vibrometric assessment of middle ear motion in Thiel-embalmed heads, *Otol. Neurotol.* **33** (3), 2012, 311–318.

Studebaker G.A., Clinical masking of air-and bone-conducted stimuli, *JSHD (J. Speech Hear. Disord.)* **29** (1), 1964, 23–35.

Stump R., Dobrev I., Krayenbühl N., Probst R. and Röösli C., In-vivo assessment of osseous versus non-osseous transmission pathways of vibratory stimuli applied to the bone and the dura in humans, *Hear. Res.* **370**, 2018, 40–52.

Thiel W., Die Konservierung ganzer leichen in natürlichen farben, *Ann. Anat.* **174** (3), 1992, 185–195.

Tonndorf J. and Khanna M., Submicroscopic displacement amplitudes of the tympanic membrane (cat) measured by a laser interferometer, *J. Acoust. Soc. Am.* **44**, 1968, 1546–1554.

~~Vasavada A.N., Li S. and Delp S.L., Three-dimensional isometric strength of neck muscles in humans, *Spine* **26** (17), 2001, 1904–1909.~~

Watanabe T., Bertoli S. and Probst R., Transmission pathways of vibratory stimulation as measured by subjective thresholds and distortion-product otoacoustic emissions, *Ear Hear.* **29** (5), 2008, 667–673.

Highlights

- Combined promontory motion shows lower intersample variation that any individual motion component.
- Contralateral promontory motion does not follow ipsilateral stimulation direction above 0.5 kHz.
- Single axis motion measurements could be overestimating the transcranial attenuation below 0.5 kHz.
- Soft-tissue stimulation could potentially provide a non-osseous pathway into the cochlea via the CSF.
- Sound propagation due to skull stimulation passes through the thicker bony sections first before activating the CSF.

Queries and Answers

Query: Please confirm that the provided email “ivo.dobrev@usz.ch” is the correct address for official communication, else provide an alternate e-mail address to replace the existing one, because private e-mail addresses should not be used in articles as the address for communication.
Answer: I confirm.

Query: Please note that author’s telephone/fax numbers are not published in Journal articles due to the fact that articles are available online and in print for many years, whereas telephone/fax numbers are changeable and therefore not reliable in the long term.
Answer: I understand.

Query: The citation "Tonndorf, 1966; Sohmer et al., 2004; Stenfelt et al., 2004; Eeg-Olofsson M et al., 2013; Hoyer and Dortheide, 1983; Dobrev at al., 2018b" has been changed to match the date in the reference list. Please check here and in subsequent occurrences.

Answer: There is no reference Stenfelt et al., 2004b - there is only one reference from that authour from that year used on this manuscript. The other changes are correct

Query: References "Reinfeldt et al., 2014" are cited in the text but not provided in the reference list. Please provide them in the reference list or delete these citations from the text.
Answer: Here is the missing reference: Reinfeldt, S., Håkansson, B., Taghavi, H. and Eeg-Olofsson, M., 2014. Bone conduction hearing sensitivity in normal-hearing subjects: Transcutaneous stimulation at BAHA vs BCI position. *International journal of Audiology*, *53*(6), pp.360-369.

Query: Have we correctly interpreted the following funding source(s) and country names you cited in your article: Swiss National Science Foundation?
Answer: Yes

Query: Please provide the volume number or issue number or page range or article number for the bibliography in Ref(s). Dobrev et al., 2018b.
Answer: Dobrev, I., Sim, J.H., Pfiffner, F., Huber, A.M. and Röösli, C., 2018. Performance evaluation of a novel piezoelectric subcutaneous bone conduction device. *Hearing research*, *370*, pp.94-104.

Query: The year in the first occurrence of Stenfelt et al., 2004 in the list has been changed to 2004a. The year in the second occurrence of Stenfelt et al., 2004 in the list has been changed to 2004b.
Answer: This repeats with the Stenfelt 2004a - delete 2004b and change 2004a to just 2004.

Query: Uncited references: This section comprises references that occur in the reference list but not in the body of the text. Please position each reference in the text or, alternatively, delete it. Any reference not dealt with will be retained in this section. Thank you.
Answer: Remove both uncited references from the reference list.

Query: Please confirm that given names and surnames have been identified correctly and are presented in the desired order and please carefully verify the spelling of all authors’ names.
Answer: Yes

Query: Your article is registered as belonging to the Special Issue/Collection entitled “ Memro 2018”. If this is NOT correct and your article is a regular item or belongs to a different Special Issue pleas contact n.bhaskaran@elsevier.com immediately prior to returning your corrections.
Answer: Yes